ANALYSIS AND COMPUTATION OF LEAKY-WAVE HYPERTHERMIA APPLICATOR

by
J R James and G Andrasic
Wolfson R.F. Eng. Centre, Royal Military College of Science, CIT
Shrivenham, Swindon, Wiltshire, SN6 8LA, UK

ABSTRACT

The use of electromagnetic waves to induce hyperthermia in cancer therapy has been the subject of intensive research but obtaining good resolution at depth in the abdomen and pelvic regions remains a fundamental problem. This paper investigates the prospects for generating leaky-waves in tissue to improve field penetration and focussing at depth. An approximate analysis based on a planar structure illustrates the feasibility of obtaining good resolution at depth but leaky-wave action in a strict sense is not possible. Measurements on an applicator conformal with the phantom tissue simulated by a saline solution, demonstrate good resolution and penetration but hotspot regions are detected around the launcher region. A three dimensional finite difference time domain (FDTD) computation is performed in Cartesian, circular cylindrical and elliptic cylindrical coordinates to model all the effects for various geometries of the phantom region and different launching symmetries. The results illustrate the need for symmetric launching of the strip, computational convergence and mode diagnostic data, the shape of focal region and the useful property of being able to shift the focal region by changing frequency. It is concluded that this new quasi-leaky-wave applicator concept is potentially capable of giving improved focal resolution at depth with some positional control and only one generator is required. Optimising the launching of the quasi-leaky-waves on the applicator and preventing hotspot regions from creating unwanted tissue heating are remaining practical problems to address.

1. INTRODUCTION

The concept of exposing tumours to electromagnetic radiation in cancer therapy has been intensively investigated in recent years [Field and Hand, 1990]. Obtaining spatial resolution of the fields at deep locations in the tissue is a fundamental problem due to the high level of loss present in the media. The heterogeneous nature of the human body, and particularly its layered nature [Hansen 1989] compound the difficulties. Direct contact applicators typically give penetration depths of a few centimetres while annular arrays enable large volumes of tissue to be heated [Turner, 1984]. The natural transverse resonance of the abdomen and pelvic regions contributes to the behaviour of the annular array and recent computer modelling [Picket-May, Taflove and Sathiaseelan, 1991] suggests that whispering gallery type modes may be an effect causing unwanted hotspots. Mutual coupling between the array apertures is also an effect to consider [Leybovich, Myerson, Emami and Straube, 1991]. The use of a large reflector antenna has been computer simulated [Chang and Mei, 1989] to demonstrate the improved spatial resolution, but no practical results are given; practical results for a microwave array focussing into the thorax region have been reported however [Melek, Anderson, Brown and Conway, 1982].Some mention has been made [Taylor, 1983, Anderson, 1986] of the possible use of inhomogeneous waves to achieve greater penetration into lossy tissue and some initial work on leaky-waves was reported by Rappaport, 1987.

The aim of this present paper is to investigate the feasibility of generating leaky-waves into lossy tissue to achieve improved spatial resolution at depths compatible with the requirements for treating tumours in the pelvic and abdomen regions. It was considered that such a leaky-wave device would offer the prospects of electronic beam scanning simply by changing the applied radio frequency. Also the fact that only one radio frequency generator is required is a distinct advantage over the annular array concept and it should also be possible to further control the focal region by electronically varying the impedance of the leaky-wave transmission line.

Several questions were however apparent at the beginning, concerning the nature of leaky-waves in a lossy medium, the launching of such waves in practice and the intensity of near fields of the launcher. It was decided that full three-dimensional computations embracing all these aspects were required and the finite

difference time domain (FDTD) method was chosen. This method is capable of accommodating heterogeneous media as presented by the human body but the scope of the present work is confined to a homogeneous phantom simulating muscle. To gain insight into the preservation of leaky-wave action in the presence of lossy media, a simplified mathematical model is derived and some experimental work has been carried out on the practical problems associated with launching leaky-waves. These latter aspects will be reported first.

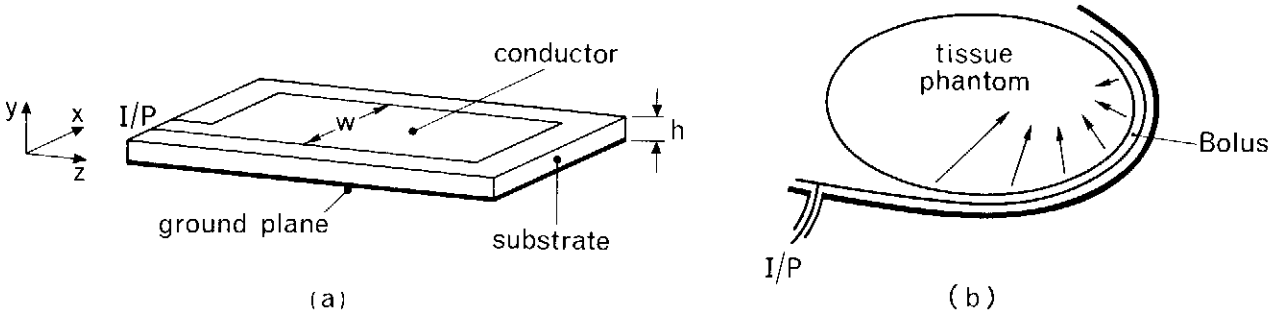

Fig 1 (a) Conventional leaky-wave microstrip antenna (b) Sectional view of microstrip structure conformal with cross-section of abdomen region and bolus.

2. APPROXIMATE ANALYSIS OF APPLICATOR

The clinical requirements suggest that a convenient form for the applicator would be a thin planar assembly in close contact with the abdomen. A suitable structure to investigate is the planar microstrip leaky-wave antenna sketched in Fig 1a, showing a conducting strip of width W on a dielectric sbstrate of thickness h backed by a conducting ground plane. This very wide microstrip line radiates leaky-waves with a narrow beamwidth when asymmetrically excited and this offers improved spatial resolution for an applicator. It was conjectured that the hyperthermic applicator would be similar in structure but bent conformally with the cross-section of the lossy abdomen into which the leaky-waves are to propagate. The spatial resolution would be further enhanced by the curvature as sketched in Fig 1b. The extent to which leaky-wave action gives improved spatial resolution depends on the degree of loss in the lossy media. For patient comfort and to avoid the burning of the abdomen skin, cooled water will be circulated in a bolus region between the applicator and the body. The length of the applicator is detemined by the extent to which the leaky-wave discharges its power as it progresses along the conducting strip.

The following approximate analysis for electrically thin substrates adopts the Wiener-Hopf analysis of Chang and Kuester, 1981, in a similar way to Oliner, 1987, with the exception that the space above the conducting strip is occupied by lossy media with a complex relative permittivity $\epsilon_{mc} = \epsilon_m - j\sigma_m/(\omega\epsilon_0)$ where $j = \sqrt{-1}$ and ϵ_0 = the free space permittivity. We use the representation in terms of a relative dielectric constant ϵ_m and conductivity σ_m. Transverse electromagnetic (TEM) waves are launched in the parallel plate substrate region between the conducting strip of width W and the ground plane. The substrate of thickness h has a complex relative permittivity $\epsilon_{rc} = \epsilon_r - j\sigma_r/(\omega\epsilon_0)$. For a narrow conducting strip, the TEM waves reflect from the strip edges to create the quasi-TEM microstrip wave used in circuits defined by a longitudinal wavenumber

$$\begin{aligned} k_z &= \beta - j\,\alpha \\ k_z^2 &= k_0^2\,\epsilon_{rc} - k_{x\epsilon}^2 \end{aligned} \tag{1}$$

where α and β are the attenuation and phase constants respectively, k_0 is the free space wavenumber and $k_{x\epsilon}$ is the leaky-wave transverse wavenumber in the substrate in the x direction; the coordinate system is given in Fig 1a. For a time dependence of $\exp(j\omega t)$, the transcendental equation relating W and mode number n is

$$\exp j(\chi - k_{x\epsilon} W) \;=\; -1 \;=\; \exp(\pm j\,n\,\pi),\; n\ odd \tag{2}$$

or

$$\chi - k_{x\epsilon} W = \pm n\pi \ , \ n \ odd$$

where

$$\chi = 2 \arctan \left[\frac{k_z}{k_{x\epsilon}} \tanh \Delta \right] - f_c \left[\frac{-k_{x\epsilon}}{k_0} \right]$$

where $k_0 h \sqrt{\epsilon_r} \ll 1$ and Δ and $f_c \left[\frac{-k_{x\epsilon}}{k_0} \right]$ are formulas given by Oliner, 1986 containing a transverse wavenumber k_x for the airspace region above the strip. $n = 0$ yields the dominant quasi-TEM microstrip mode while $n = 1$ is the first leaky-wave mode and the one we wish to generate. This mode has an electric field tangential to the strip in the airspace. For odd modes a vertical electrical wall exists mid-way beneath the strip in the y direction while the even modes have a magnetic wall.

To convert the analysis to the present case where the airspace is replaced by lossy tissue we assert that

$$k_x^2 = k_0^2 \epsilon_{mc} - k_z^2 \tag{3}$$

In the absence of lossy media above the strip leaky-waves exist for $\alpha > 0$ and $\beta < k_0$ which is associated with electrically wide strips. The presence of losses will rapidly attenuate the leaky-waves and we have previously referred to this action as a quasi-leaky-wave (Andrasic, James and Hand, 1990, 1991 a and b) and shown that improved spatial resolution is still possible and is superior to that produced by a conventional type of applicator. The choice of frequency is illustrated for planar applicators in Fig 2 for the $n = 1$ mode. We seek the condition where the phase shift along the z direction is small and α is neither too large to leak the power prematurely nor too small to enable the power to be transferred to the tissue. The planar structure in Fig 2 is similar to that in Fig 1a except that the space above the strip is occupied by lossy tissue with constants ϵ_m and σ_m . The substrate is low loss water. A change of frequency will cause the focal field point to move in position with some defocussing

To calculate the electrical field E(P) at a point P within the elliptical shaped homogeneous phantom of complex relative permittivity ϵ_{mc} it is assumed that the modal conditions on the planar structure are largely maintained when it is bent conformal with the phantom.

$$E(P) = -\Delta \times F$$

$$F = \frac{\epsilon_{mc}}{2\pi} \int_{\phi=\phi_1}^{\phi_2} J_M \left[\frac{\exp(-jkR_1)}{R_1} + \frac{\exp(-jkR_2)}{R_2} \right] ds(\phi) \tag{4}$$

where J_M is the equivalent magnetic current around the edges of the conducting strip and $k = k_0 \sqrt{\epsilon_{mc}}$

$$J_M = \exp\left[-j(\beta - j\alpha)\, s(\phi)\right] \tag{5}$$

R_1 and R_2 are the distances from the current elements $ds(\phi)$ at each strip edge to point P and the angle ϕ rotates about the central axis of an elliptical phantom as J_M is integrated along the extent of the strip. The specific absorption rate (SAR) defines the hyperthermic heating effect within tissue and for the homogeneous phantom region is proportional to $| E(P) |^2$. The computed SAR result in Fig 3a substantiates the expectations showing a good spatial resolution at a depth of some 8cms into the phantom and its positional variability with frequency. The phantom conductivity is for the saline solution used and is lower than that in Fig 2 caption.

3.EXPERIMENTAL RESULTS

The main purpose here is to investigate how to connect the coaxial cable from the generator to the applicator to ensure that the $n = 1$ mode is generated with little $n = 0$ contribution and the minimum of unwanted hotspots around the launcher region. Saline solution (3gms/litre) with $\epsilon_{mc} = 76 - j150$, ($\sigma_m = 6 \times 10^{-3}$ S/cm)

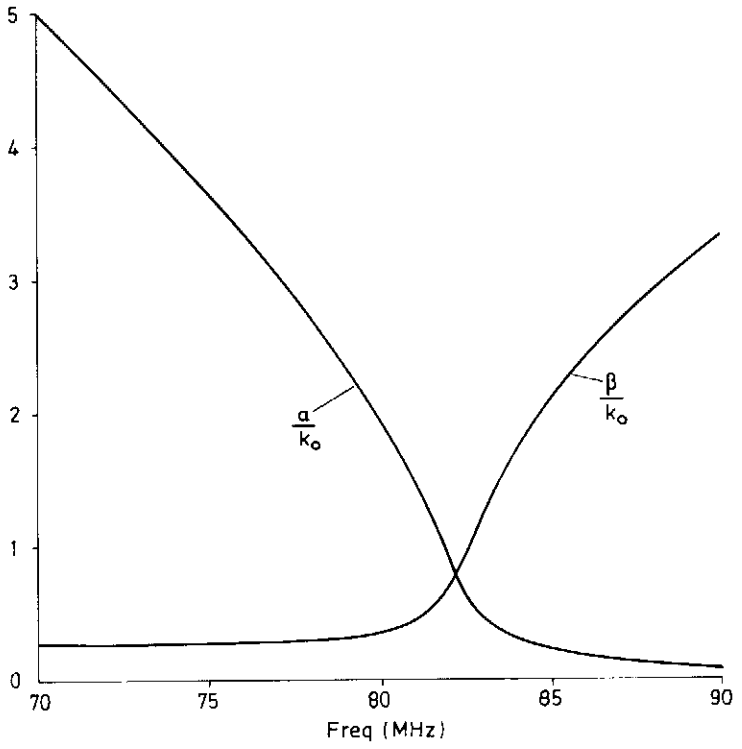

Fig 2 α and β values for planar structure for n = 1 mode eqns(1-3);
$W = 20$ cms, $h = 1$ cm, $\epsilon_r = 76$, $\sigma_r = 6 \times 10^{-5}$ S/cm, $\epsilon_m = 76$, $\sigma_m = 8 \times 10^{-3}$S/cm

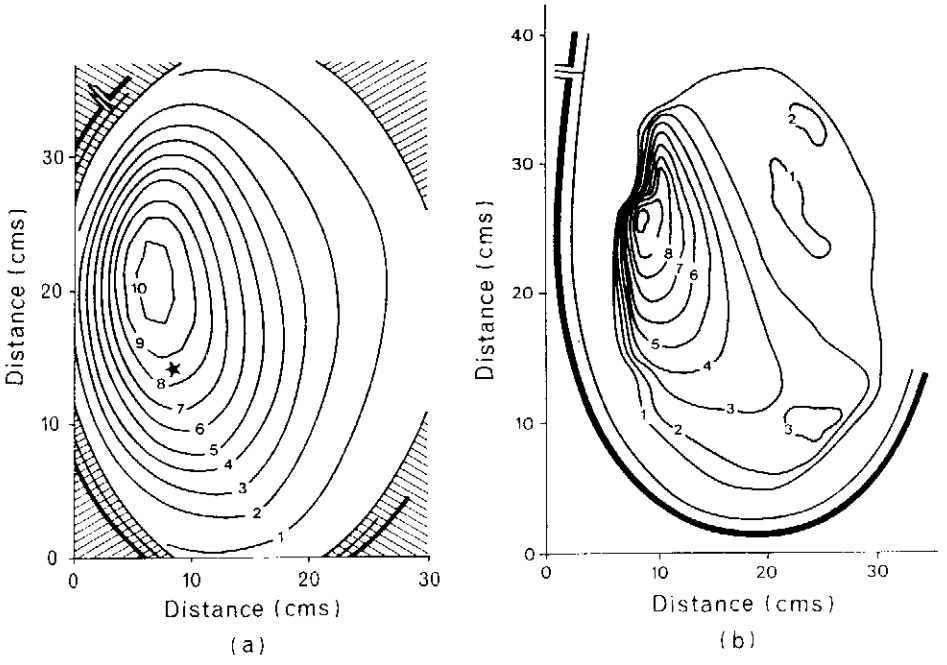

Fig 3 Relative Specific Absorption Rate (SAR) contours with linear increments, within the elliptical phantom with major and minor axis of 39.5cm and 31.5cm respectively, at 72MHz, in central transverse plane. Electrical constants as in Fig 2 caption, except that $\sigma_m = 6 \times 10^{-3}$ S/cm.

(a) Computed eqns (1) to (5). At 82MHz focal region shifts to starred location.

(b) Probe measurement of SAR corresponding to dominant electric field in direction of ellipse axis.

was used as the phantom held in a polythene container; Fig 4a illustrates the bolus region and surrounding water which will assist patient comfort. The field scanning monopole probe, the phantom container and the applicator ground plane can be seen in the corresponding photograph, Fig 4b. The coaxial cable was attached to one corner of the conducting strip of width W chosen to reject modes for $n > 1$ in the planar version and a typical measurement, Fig 3b, is in reasonable agreement with the approximate analytical result. The input region is bent away from the phantom as in Fig 1b to facilitate probing of the fields. When the input field region was probed, field hotspots were detected around the launcher and furthermore the focal region showed little shift with frequency. Attempts at constructing a balanced launcher using two coaxial cable inputs of opposite polarity had some effect on the shape of the focal region, but the launcher hotspots persisted. The field perturbation created by the monopole probe and the corrosive effects of the saline solution, are some of the limitations that prevented an accurate quantification of these effects.

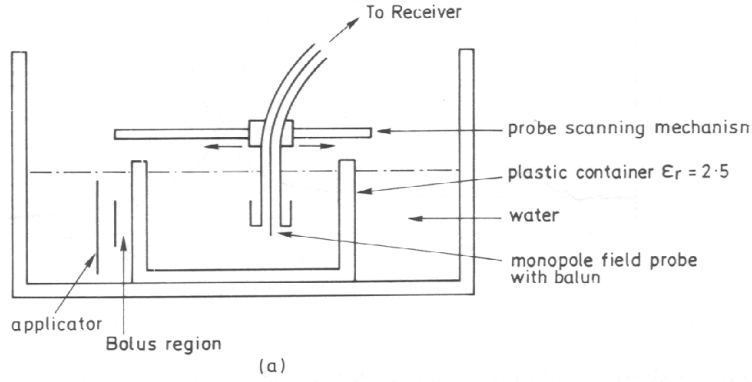

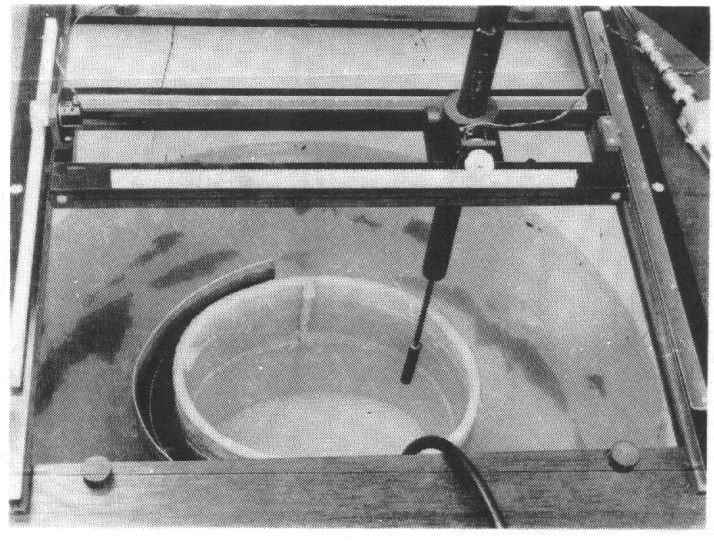

(b)

Fig 4 Experimental rig.

(a) Sketch of cross-section of elevation view showing phantom and the surrounding water.

(b) Photograph showing part of applicator pulled away from the container of phantom for the purposes of viewing.

4. FINITE DIFFERENCE TIME DOMAIN (FDTD) COMPUTATION

4.1 Planar Geometry

To investigate the likely resolution benefits described in section 2 we consider a planar version of the applicator as sketched inset in Fig 6. In the FDTD programming on a VAX 8800, the basic method of Yee, 1966 is adopted throughout. The planar structure shown inset in Fig.6 is resolved into cube cells of 1cm sides, having assigned values of permittivity, permeability and boundary conditions. The region between the conducting strip and ground plane has $h = 1$ cm and thus are one cell deep. In all, 63000 cells were allocated to a rectangular lattice of $30 \times 30 \times 70$ which embraced the applicator, and the lossy tissue of complex permittivity ϵ_{mc} above the conducting strip. In addition buffer regions each occupying $10 \times 30 \times 70 = 21000$ cells were placed on both sides of the lattice, thus there were 105000 cells in the computational domain. Absorbent boundary conditions based on the equations of Mur 1981, were placed at the extremes of the computational domain. A transient sinusoid was applied to one corner of the conducting strip for asymmetric excitation and antiphase transient sinusoids at each corner for symmetric excitation. The formulation of Maxwell's equation in differential form in terms of spatial increments Δx, Δy, Δz and the time step Δt together with the leap-frogging process and numerical stability condition follows the conventional methods [Yee, 1966, Sheen, Ali, Abouzahra, and Kong, 1990].

An example of the FDTD computation in Fig. 5 shows the steady state achieved at 81 MHz after 700 time steps. With asymmetric launching there will be some $n = 0$ TEM mode present and the decomposition in Fig. 5 quantifies this. Examination of the SAR in the phantom region Fig. 6, illustrates the undesirable standing wave patterns due to the presence of both $n = 0$ and $n = 1$ modes when asymmetrically excited. The symmetric excitation case is readily computed by inserting a central electric wall as previously mentioned. The SAR corresponding to the dominant E_x component is plotted in Fig. 7 and a well resolved focal region is achieved at a height of approximately 7cm above the conducting strip. The result in Fig 7 shows the ideal situation where only the $n = 1$ mode exists but in practice the launching of the latter will create field concentrations and other hotspot regions. Clearly improved resolution depends on the success in launching the $n = 1$ mode with the minimum launcher disturbance. The presence of a lossless bolus layer between the conducting strip and phantom has insignificent effect and is also omitted in these computations.

4.2 Curvilinear Geometry

There is evidence [Harms, Lee and Mittra, 1992] that the body fitting of cells in the FDTD method has an influence on convergence and accuracy. For this reason we have recast the FDTD formulation in curvilinear coordinates having greater geometrical compatibility with the phantom shape, to achieve improved resolution of the hotspots particularly in the launcher region. Both circular and elliptic cylindrical coordinate lattices have been developed as shown in Fig 8a and b respectively. For circular cylindrical geometry the Maxwell's equations in differential form in ρ, ϕ, z coordinates are given as,

$$\frac{\partial H_z}{\partial t} = -\frac{1}{\mu\rho}\left[\frac{\partial(\rho E_\phi)}{\partial \rho} - \frac{\partial E_\rho}{\partial \phi}\right]$$

$$\frac{\partial E_z}{\partial t} = \frac{1}{\epsilon}\left[\frac{1}{\rho}\left\{\frac{\partial(\rho H_\phi)}{\partial \rho} - \frac{\partial H_\rho}{\partial \phi}\right\} - \sigma E_z\right]$$

which may be represented in difference form as,

$$\begin{aligned} H_z^{n+1/2}(i+1/2, j+1/2, k) = {} & H_z^{n-1/2}(i+1/2, j+1/2, k) \\ & + \frac{\Delta t}{\mu\rho}\{[E_\rho^n(i+1/2, j+1, k) - E_\rho^n(i+1/2, j, k)]/\Delta\phi + \\ & [\rho_i E_\phi^n(i, j+1/2, k) - \rho_{i+1} E_\phi^n(i+1, j+1/2, k)]/\Delta\rho\} \end{aligned}$$

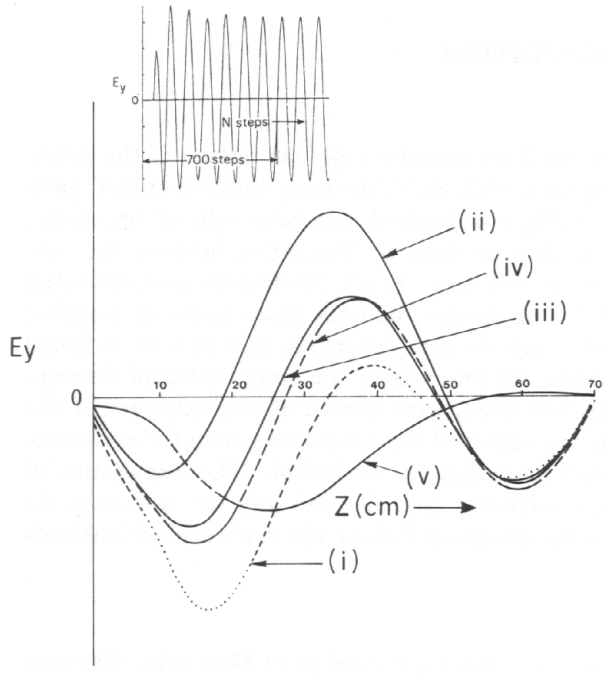

Fig 5 FDTD computation of E_y field at 81MHz and decomposition into symmetric and asymmetric modes. Electrical constant and lattice extent are as in Fig 6. E_y field reaching steady-state after 700 time steps is shown inset.

(i) and (ii) Fields of edges of strip
(iii) TEM field calculated from ((i) + (ii))/2
(iv) TEM field at centre of strip
(v) n = 1 mode at one edge calculated from ((i) - (ii))/2

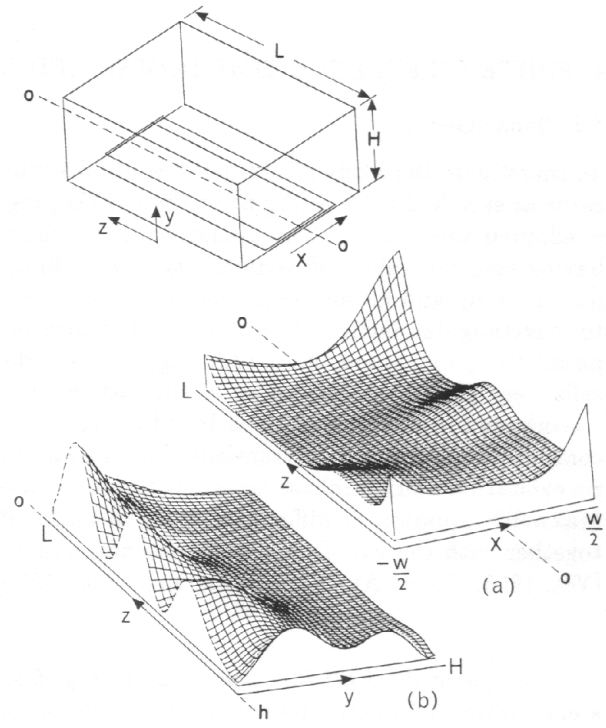

Fig 6 Computed plots of relative Specific Absorption Rate (SAR) levels at 81MHz for asymmetrically excited planar strip with $W = 20$ cm, ground plane width = 30 cm, $h = 1$ cm, $H = 30$ cm, $L = 70$ cm, $\epsilon_r = 76$, $\epsilon_m = 76$, $\sigma_r = 6 \times 10^{-5}$ S/cm, $\sigma_m = 6 \times 10^{-3}$ S/cm. Sketch of applicator is shown inset.

(a) $| E_x |^2$ at height y = 10 cm
(b) $| E_x |^2$ in yz plane at x = 0

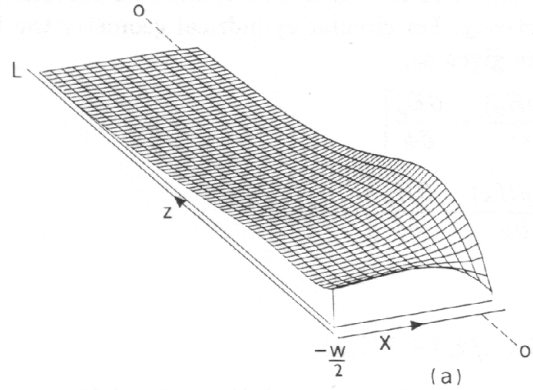

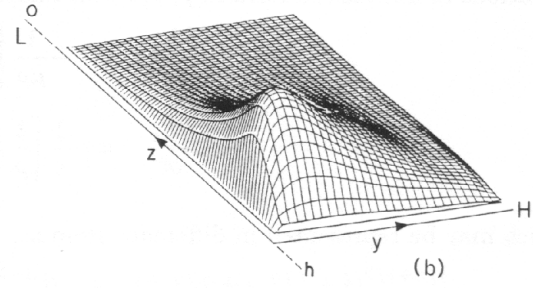

Fig 7 Computed plots of relative Specific Absorption Rate (SAR) levels as in Fig 6, but symmetrical excitation enforced by central electric wall.

(a) $| E_x |^2$ at $y = 10$ cm
(b) $| E_x |^2$ in yz plane at $x = 0$

$$E_z^{n+1}(i,j,k+1/2) = \left(\frac{1-S}{1+S}\right) E_z^n(i,j,k+1/2)$$
$$+\frac{\Delta t}{\epsilon(1+S)}\{[H_\rho^{n+1/2}(i,j-1/2,k+1/2) - H_\rho^{n+1/2}(i,j+1/2,k+1/2)]/\Delta\phi +$$
$$[\rho_{i+1/2}H_\phi^{n+1/2}(i+1/2,j,k+1/2) - \rho_{i-1/2}H_\phi^{n+1/2}(i-1/2,j,k+1/2)]/\Delta\rho\}$$

where $S = \sigma\Delta t/(2\epsilon)$ and $\rho_i = i \times \Delta\rho$

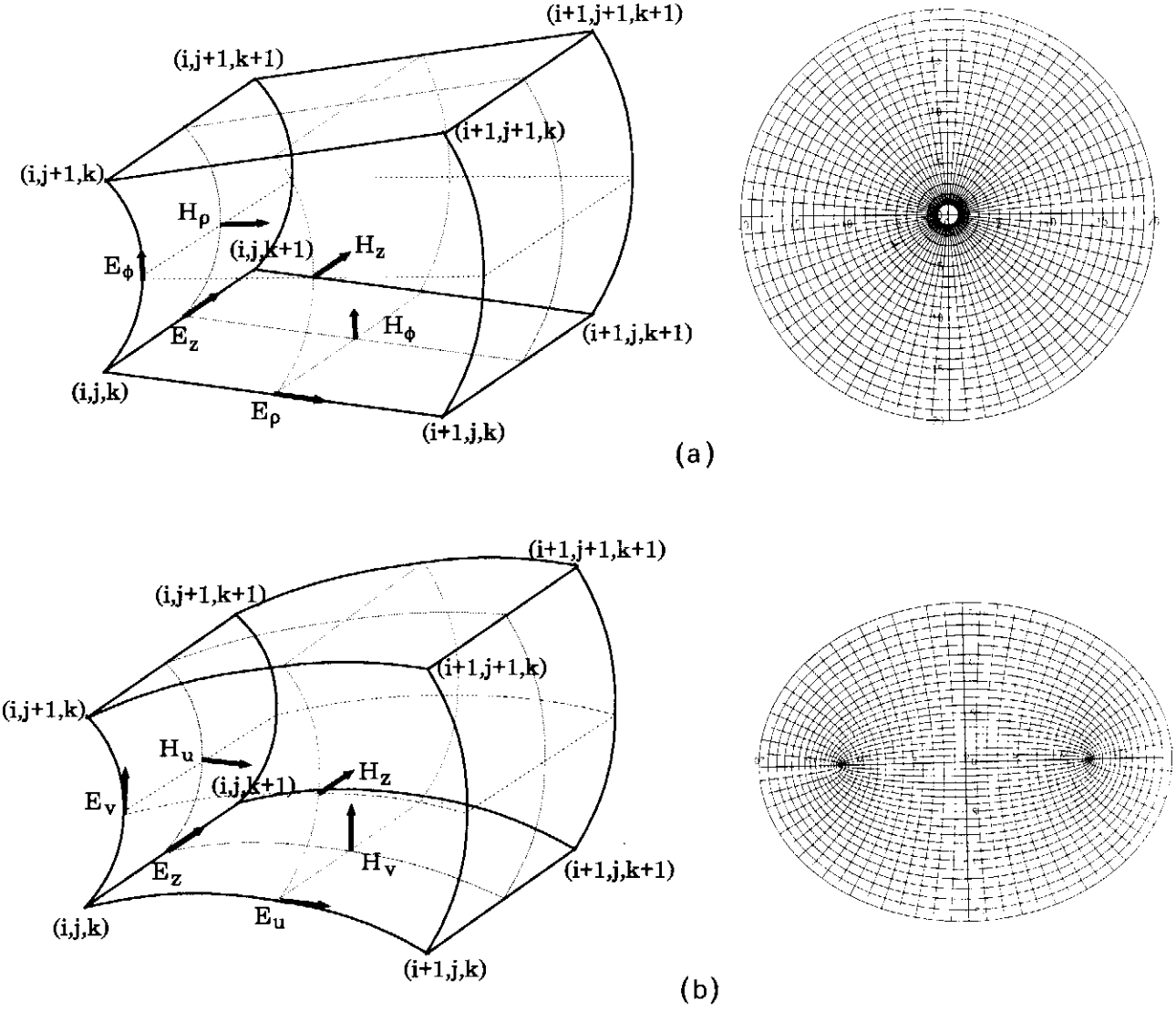

Fig 8 Geometry of leapfrogging unit cell and corresponding lattice for curvilinear coordinates
(a) circular cylinder coordinates
(b) elliptic cylinder coordinates

Mur's Absorbing boundary condition is applied in the plane boundaries at $z = 0$ and z_L which are the extreme planes of the computational domain. A perfectly conducting boundary surface is assumed at the circular boundary corresponding to an extended ground plane.

A similar set of equations were obtained for the elliptic cylinder case, where the coordinates u, v, and z were used and the corresponding difference equations are given by

$$\begin{aligned} H_z^{n+1/2}(i+1/2, j+1/2, k) &= H_z^{n-1/2}(i+1/2, j+1/2, k) \\ &+ \frac{\Delta t}{\mu h^2}\{[h_{j+1}E_u^n(i+1/2, j+1, k) - E_u^n(i+1/2, j, k)]/\Delta v + \\ &[h_i E_v^n(i, j+1/2, k) - h_{i+1}E_v^n(i+1, j+1/2, k)]/\Delta u\} \end{aligned}$$

$$\begin{aligned} E_z^{n+1}(i, j, k+1/2) &= \left(\frac{1-S}{1+S}\right) E_z^n(i, j, k+1/2) \\ &+ \frac{\Delta t}{\epsilon(1+S)h^2}\{[H_u^{n+1/2}(i, j-1/2, k+1/2) - H_u^{n+1/2}(i, j+1/2, k+1/2)]/\Delta v + \\ &[h_{i+1/2}H_v^{n+1/2}(i+1/2, j, k+1/2) - h_{i-1/2}H_v^{n+1/2}(i-1/2, j, k+1/2)]/\Delta u\} \end{aligned}$$

where $S = \sigma\Delta t(2\epsilon)$ and $h = d\sqrt{\cosh u^2 - \cos v^2}$, $h_i = d\sqrt{\cosh(i\Delta u)^2 - \cos v^2}$, d being the distance between the foci of the ellipse.

For the circular case the cell size is defined by $\Delta r = 1$ cm, $\Delta\phi = 5^o$ and $\Delta z = 1$ cm and in the r ,ϕ and z directions these are respectively $20 \times 72 \times 30 = 43200$ cells encompassing the circular shaped applicator and phantom. The latter is sandwiched between buffer regions comprised of phantom material and each buffer region has, in the r , ϕ and z directions respectively $20 \times 72 \times 10 = 14400$ cells. The total number of cells in the computational domain is thus 72000 cells where $z_L - z_0 = 50\Delta z$. In elliptic geometry the cell structure in u, v and z coordinates is similarly organised with 43200 cells comprised of a central lattice containing the applicator and 28800 cells for the two adjacent buffer regions.

The six SAR results in Fig 9a to f compare FDTD computations with the approximate analysis eqn(4), illustrating the effect of circular and elliptic phantom geometry and the shift of the focal region with frequency in the range 75 to 82 MHz. The applicator is conformal with the phantom geometry and the circular phantom has a smaller cross-sectional area than the elliptic shaped phantom. Launcher hotspots in this central transverse plane of the phantom lie just outside the contour regions shown. The FDTD results Fig 9b at 75MHz shows a similar size focal region as the approximate analysis Fig 9a some 7cms deep. Altering the frequency to 82MHz certainly gives a worthwhile shift in the focal region's position Fig 9d and again the analytical results Fig 9c has a similar focal resolution but is more elongated. This is likely to be due to the various assumptions made in the analysis, but is otherwise seen as encouraging agreement in predicting the fundamental behaviour. The elliptical cases Figs 9e and f shows similar characteristics and, as may be anticipated, the focal region is more elongated. The distortion in the FDTD contours Fig 9f was found to be due to the excessive cell length near the elliptic focii.

It was found that the presence of hotspots around the launcher region, and to a lesser extent at the terminal end of the conducting strip, were greatly influenced by the phantom boundary diametrically opposite to the applicator. An example is given in Fig 10a for a circular phantom at 75 MHz where the hotspot regions near the launcher and terminal end of applicator are more pronounced than the desired focal region. The region outside the circular phantom is occupied by water and when the conductivity is increased to that of the phantom the hotspots are less prominent Fig 10b and one inference is that reflections are occurring in the configuration of Fig 10a at the phantom/water interface which disturb the launching process. In Fig 10c the water exterior to the phantom is made more conducting than the phantom and the hotspots become negligible suggesting that there are no reflections from the phantom boundaries. Finally FDTD computations in other than the central transverse plane indicate that the field markedly decreases but remains large near the edge of the conducting strip.

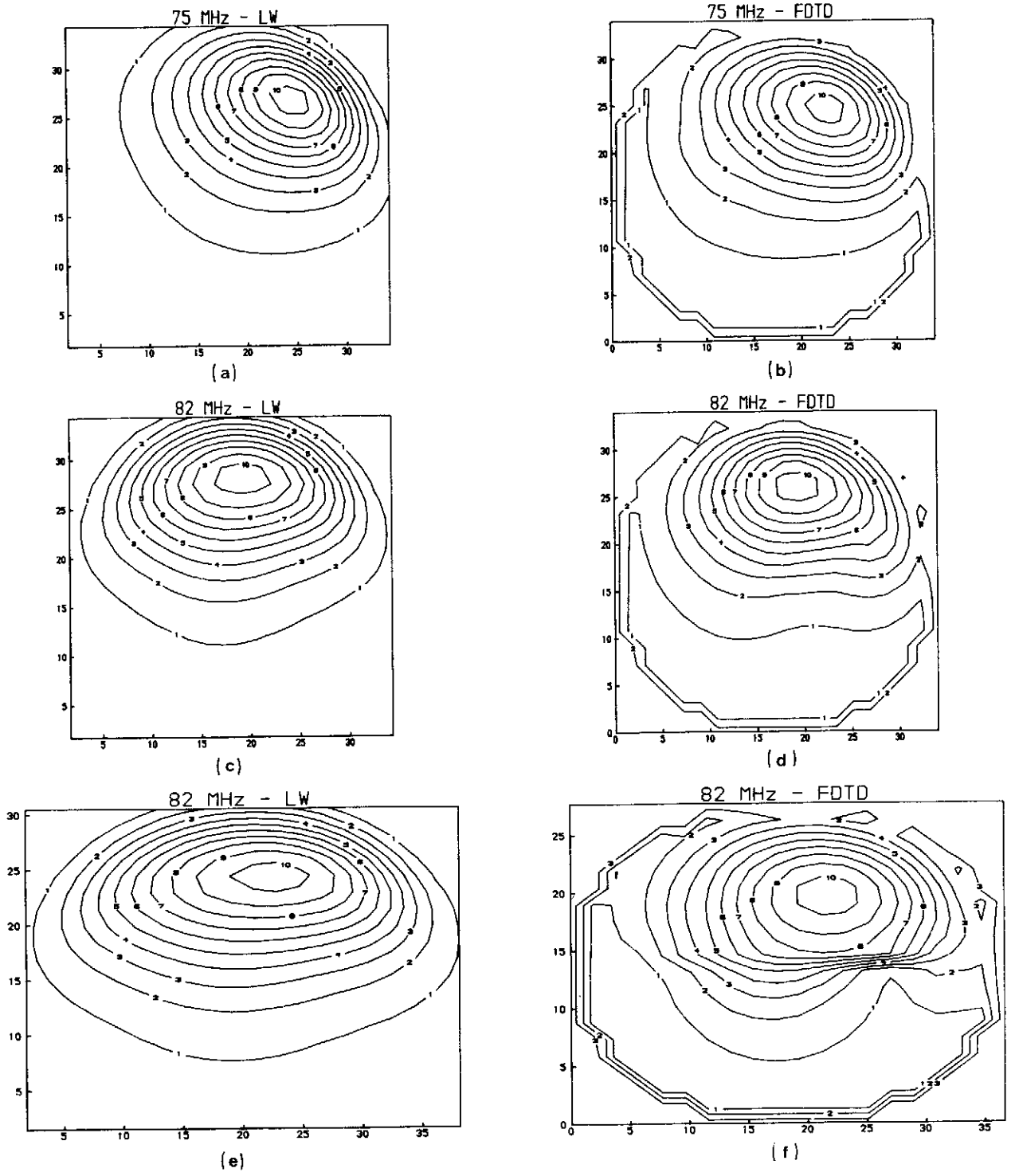

Fig 9 Computed relative Specific Absorption Rate (SAR) levels using approximate leaky-wave (LW) analysis eqns (1) - (5) and FDTD method. No bolus incorporated and $\epsilon_m = 76, \sigma_m = 6 \times 10^{-3}$ S/cm. Contour relative levels are on a linear scale with maximum of 10.

(a) LW at 75MHz
(b) FDTD at 75MHz
(c) LW at 82MHz
} circular phantom diameter = 38 cm

(d) FDTD at 82MHz
(e) LW at 82MHz
(f) FDTD at 82MHz
} elliptical phantom as defined in Fig 3 caption

At the phantom boundary, curves fragment due to interpolation routine used.

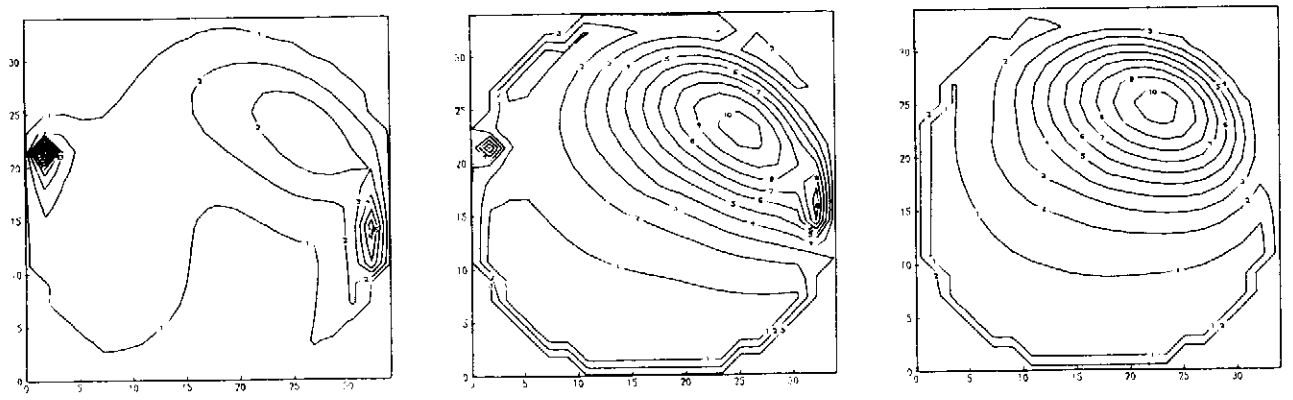

Fig 10 Examination of hotspots in computed 75MHz relative Specific Absorption Rate (SAR) levels using FDTD method. Contour relative levels are on a linear scale with maximum of 10.and electrical data for circular phantom is given in Fig 9 caption. The circular phantom is bounded by the square frame. Water at the phantom/water interface has the following loss.

(a) 6×10^{-5} S/cm
(b) 6×10^{-3} S/cm
(c) 6×10^{-1} S/cm

5. DISCUSSION AND CONCLUSION

The combination of FDTD computations and independent approximate analysis together with some limited experimental results, confirm that a quasi-leaky-wave can be excited in a homogeneous tissue phantom using a wide microstrip-type applicator conformal with the phantom. The approximate analysis usefully highlights the need for a means of launching only the quasi-leaky-wave mode, since a TEM presence will not release the power to the phantom with the same focal resolution and standing waves will occur. These effects and the need for symmetric excitation of the strip is confirmed by FDTD computation of a planar version of the applicator. Unwanted hotspot regions around the launcher and the terminal end of the applicator have been examined by recasting the FDTD computations in curvilinear form and examples for both circular and elliptic cylindrical phantoms are given. It is considered that with greater computer capacity and speed it would have been sufficient to work with cube Cartesian lattices throughout, but the experience with the curvilinear version has proved of interest and in the elliptical case has posed difficulties. The presence of a lossless bolus region appears not to diturb the overall behaviour. The FDTD method is ideally suited to layered and other heterogeneous media as presented by realistic tissue and this has been outside of the present study.

The results of this study suggest that the quasi-leaky-wave applicator concept is potentially useful, offering good focal resolution at a depth that could be particularly useful in the abdominal and pelvic regions. The use of one generator and a frequency scanned beam are added advantages, but the development of such a device would demand attention to the hotspot behaviour, design of a symmetric launching system, the possible sensitivity of the focal region to tissue characteristics and a means of accommodating a variety of patient dimensions. Mode filters might be usefully incorporated in the conducting strip to assist the launching process. It is also possible that the launcher region could be offset from the tissue as sketched in Fig 1b and additional cooling applied to hotspot regions. The hotspot behaviour also appears to be sensitive to absorbent loading at the tissue/water interface and this needs further investigation.

In conclusion the analytical, computational and experimental work has confirmed the potentially useful properties of quasi-leaky-wave generation in hyperthermia cancer treatment and issues requiring further investigation have been identified.

6.ACKNOWLEDGEMENTS

The authors are very grateful to Dr J W Hand MRC, Hammersmith Hospital, London, UK for helpful discussion and advice. The research was supported by the Medical Research Council, UK.

7.REFERENCES

ANDERSON, J. BACH, 1986, Regional electromagnetic heating, in Physical Techniques in Clinical Hyperthermia (Edited by J W Hand and J R James) (Research Studies Press, distributed by John Wiley and Sons Inc. Chichester pp71 - 73.

ANDRASIC, G., JAMES, J.R., and HAND, J.W., 1990, Quasi-leaky-wave applicator for deep heating, 11th ESHO Conference, Latina, Italy, Sept 17-20, Abstract published in Strahlenther, Onkol. 166(1990), p506, Nr. 8.

ANDRASIC, G., JAMES, J.R., and HAND, J.W., 1991a, Investigation of quasi-leaky-wave applicator using FD-TD computations, Proc IEE Inter. Conf. on Antennas and Propagation, York, England, 15-18 April, pp584 - 587.

ANDRASIC, G., JAMES, J.R., and HAND, J.W., 1991b, FDTD computation of leaky-wave behaviour in electromagnetic induced hyperthermia, Progress in Electromagnetics Research Symposium, Cambridge, Mass, USA, 1-5 July, abstract p568.

CHANG, D.C., and KUESTER, E.F., 1981, Total and partial reflection from the end of a parallel-plate waveguide with an extended dielectric loading, Radio Science, 16, Jan-Feb, pp1 - 3.

CHANG, H.C., and MEI, K.K., 1989, A Computer simulation of using a large reflector antenna for microwave hyperthermia, Proc ISAP, Aug, Tokyo, Japan, pp 261-264.

FIELD, S.B., and HAND, J.W., (Editors), 1990, An introduction to the practical aspects of clinical hyperthermia, (London Taylor and Francis).

HANSEN, V.W., 1989, Numerical solution of antennas in layered media, (Research Studies Press, distributed by John Wiley and Sons Inc, Chichester, England)

HARMS,P.H., LEE, J-F. and MITTRA, R., 1992, A study of the non-orthogonal FDTD Method versus the conventional FDTD technique for computing resonant frequencies of cylindrical cavities, IEEE Trans. on Microwave Theory and Techniques, vol 40, No 4, April, pp 741-746.

LEYBOVICH, L.B., MYERSON, R.J., EMAMI, B. and STRAUBE, W.L., 1991, Evaluation of the Sigma 60 applicator for regional hyperthermia in terms of scattering parameters, Intl. Jour. Hyperthermia, vol 7, No 6, pp 917-935.

MELEK, M. ANDERSON, A.P., BROWN, B.H. and CONWAY, J., 1982, Measurements substantiating localised microwave hyperthermia within a thorax phantom, Electron. Lett., 18, pp437 - 438.

MUR, G., 1981, Absorbing boundary conditions for the finite difference approximation of the time-domain electromagnetic field equations, IEEE Trans. Electromag. Compat., Vol EMC - 23, pp377 - 382.

OLINER, A.A., 1986, Scannable millimeter wave arrays, Mid-period report on RADC Contract No F19628-84-K.0025, Polytechnic Institute of New York, USA.

OLINER, A.A., 1987, Leakage from higher modes on microstrip line with applications to antennas, Radio Science, vol 22, No 6, November, pp 907-912.

PICKET-MAY, M.J. TAFLOVE, A., and SATHIASEELAN, V, 1991, FD-TD computational modelling of electromagnetic hyperthermia, Proceedings of PIERS, Cambridge, USA, July 1-5, p113.

RAPPAPORT, C.M. MORGENTHALER, F.R. and LELE, p.p.. 1987, Experimental study of the controllable microwave trough guide applicator, Jour, Microwave Power and Electromagnetic Energy (USA), Vol 22, No 2., pp77 - 78.

SHEEN, D.M. ALI, S.M. ABOUZAHRA, M.D. and KONG, J.A., 1990, Applicator of the three-dimensional finite-difference time-domain method to the analysis of planar microstrip circuits, IEEE Trans. and Microwave Theory and Techniques, Vol 38, No 7, July, pp849-857.

TAYLOR, L.S., 1983, Therapeutic applications of electromagnetic heating, Proc IEE Inter. Conf. on Antennas and Propagation, York, England, 12-15 April, pp425 - 431.

TURNER, P.F., 1984, Regional Hyperthermia with an annular phased array, IEEE Trans, Biomed. Eng, Vol BME-31, No 1, Jan, pp106 -114.

YEE, K.S., 1966, Numerical solution of initial boundary value problems involving Maxwell's equations in isotropic media, IEEE Trans. Antennas and Prop., Vol AP-14, pp302 - 307.